AGU ADVANCING EARTH AND SPACE SCIENCE

Geophysical Research Letters

RESEARCH LETTER
10.1029/2020GL090530

A Paleoseismic Record Spanning 2-Myr Reveals Episodic Late Pliocene Deformation in the Western Qaidam Basin, NE Tibet

Yin Lu[1,2,3], Shmuel Marco[4], Nadav Wetzler[5], Xiaomin Fang[6,7], G. Ian Alsop[8], and Aurélia Hubert-Ferrari[2]

[1]Institute of Earth Sciences, Heidelberg University, Heidelberg, Germany, [2]Department of Geography, University of Liège, Liège, Belgium, [3]Department of Geology, University of Innsbruck, Innsbruck, Austria, [4]Department of Geophysics, Tel Aviv University, Tel Aviv, Israel, [5]Geological Survey of Israel, Jerusalem, Israel, [6]Key Laboratory of Continental Collision and Plateau Uplift, Institute of Tibetan Plateau Research, Chinese Academy of Sciences, Beijing, China, [7]CAS Center for Excellence in Tibetan Plateau Earth Sciences, Chinese Academy of Sciences, Beijing, China, [8]Department of Geology & Geophysics, University of Aberdeen, Scotland, UK

Key Points:

- We interpret micro-faults, soft-sediment deformation, slumps, and detachment surfaces as paleoearthquake/tectonic indicators
- The core records five seismite clusters between 3.6 and 2.7 Ma, revealing episodic thrusting in relation to intense regional deformation
- During the clusters, regional deformation was concentrated more in the fold-and-thrust system than along regional major strike-slip faults

Supporting Information:

- Supporting Information S1

Correspondence to:

Y. Lu,
Yin.Lu@uibk.ac.at;
yinlusedimentology@yeah.net

Citation:

Lu, Y., Marco, S., Wetzler, N., Fang, X., Alsop, G. I., & Hubert-Ferrari, A. (2021). A paleoseismic record spanning 2-Myr reveals episodic late Pliocene deformation in the western Qaidam Basin, NE Tibet. *Geophysical Research Letters*, *48*, e2020GL090530. https://doi.org/10.1029/2020GL090530

Received 27 AUG 2020
Accepted 22 JAN 2021

Abstract The western Qaidam Basin, NE Tibet contains numerous NW-SE-trending thrusts that extend over a distance of ~300 km along the Altyn Tagh Fault and north of the Kunlun Range. However, little is known about the long-term seismo-tectonic evolution of this active thrust zone due to the absence of an extended paleoseismic record. We present a 2-Myr-long disturbance record established from a core drilled on the crest of a thrust-cored anticline. Based on detailed sedimentological analysis, the disturbances (micro-faults, soft-sediment deformation, slumps, and detachment surfaces) are interpreted as paleoearthquake/tectonic indicators. The core records five seismite clusters which occurred at 3.6-3.5, 3.4-3.2, 3.15-3.1, 3.0-2.9, and 2.8-2.75 Ma. This suggests the rate of tectonic strain accommodated by the folds and thrusts in the region varies and thus reveals episodic local deformation. During the clusters, regional deformation is concentrated more in the fold-and-thrust system than along regional major strike-slip faults.

Plain Language Summary The generally NW-SE-trending thrusts developed north of the Kunlun Range are the most prominent morphological feature in the western Qaidam Basin, NE Tibet. These folds have played a key role in the Miocene-Quaternary uplift of the region. However, little is known about the long-term rupture behavior of this active thrust zone due to the absence of an extended paleoseismic record. Our understanding of earthquake history is still limited by short seismological and historical records. A continuous lacustrine sedimentary sequence (~33-1.6 Ma) accumulated in the Qaidam paleolake which may have sequentially recorded the development and activities of the underlying folds and thrusts. Here, we present a unique record of disturbance spanning 2-Myr based on a deep core drilled on the crest of one such fold in the western Qaidam Basin. The disturbances comprise micro-faults, soft-sediment deformation, slumps, and detachment surfaces. We interpret the four types of disturbance as seismites. The 2-Myr-long seismite sequence records five paleoseismic clusters that occurred between 3.6 and 2.7 Ma, suggesting episodic late Pliocene deformation in the western Qaidam Basin, NE Tibet.

1. Introduction

The Qaidam Basin is the largest topographic depression on the Tibetan Plateau and was formed since the early Oligocene by the ongoing India-Asia collision (Yin et al., 2008). It is bound to the northwest by the Altyn Tagh Range, to the south by the Kunlun Range, and the Qilian Range to the northeast (Figure 1) (Tapponnier, 2001; Taylor & Yin, 2009; Yin et al., 2008). The northeastward growth of Tibet during the Oligocene-Quaternary, and the associated propagation of deformation along the Kunlun Fault, formed a series of sub-parallel NW-SE-trending folds over a distance of ~300 km along the Altyn Tagh Fault, which is the most prominent morphological feature in the Qaidam Basin of NE Tibet (Lu et al., 2018; Métivier et al., 1998; Meyer et al., 1998; Yuan et al., 2013) (Figure 1). However, the absence of protracted paleoseismic records means that little is known about the long-term rupture behavior of the still active thrust zone.

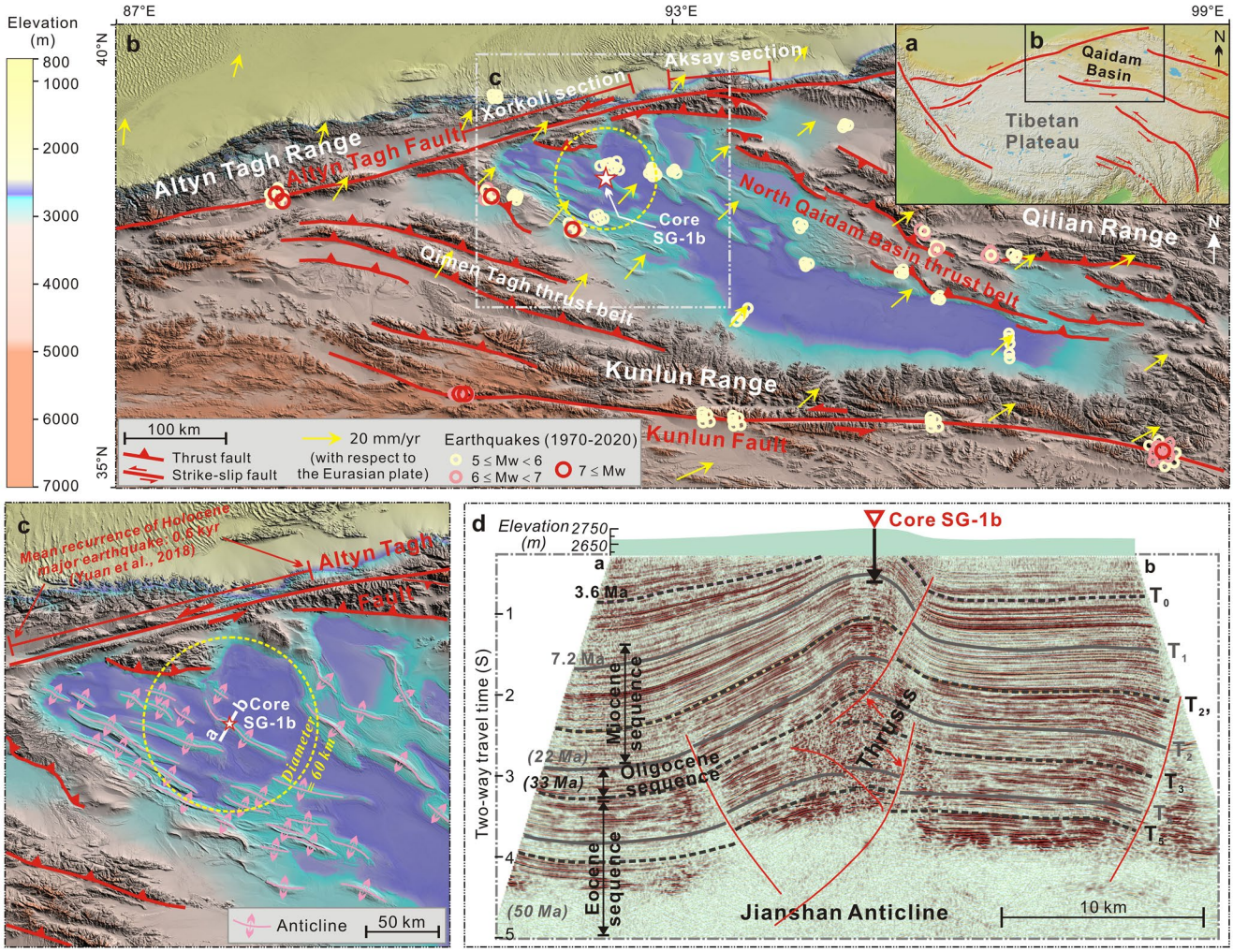

Figure 1. Geological setting of the study area. (a) Location of Qaidam Basin and major faults on the Tibetan Plateau (Tapponnier, 2001; Taylor & Yin, 2009). (b) Active faults (Cowgill et al., 2009; Taylor & Yin, 2009) and GPS velocity (Wang & Shen, 2020) in the region; circles represent earthquakes during the years 1970–2020 (http://ds.iris.edu/ds/). (c) Anticlines surrounding Core SG-1b (Taylor & Yin, 2009). (d) Seismic profile (line a–b in Figure 1c) across the Jianshan Anticline (modified from Lu et al., 2015).

Folds that trend with a 30°–45° obliquity to major strike-slip faults also occur in association with the San Andreas Fault (Miller, 1998), the Dead Sea Fault (Freund, 1965), and the North Anatolian Fault (Hubert-Ferrari et al., 2002). Their formation can be explained by the same stresses that drive the strike-slip motion, where the maximum horizontal compressive stress (S_{Hmax}) is perpendicular to the fold axes. In the case of the Qaidam Basin, the NE-SW S_{Hmax} triggers sinistral motion along both the Altyn Tagh Fault and the Kunlun Fault. This study aims to characterize the seismo-tectonic evolution of an anticline within the Qaidam Basin, which can promote further understanding of strain partitioning in the vast deformation zone related to the Indo-Asia collision.

Earthquakes trigger various types of deposits and structures, also known as seismites (Seilacher, 1969), and include micro-faults (Avşar et al., 2016; Monecke et al., 2004), soft-sediment deformation (Jackson et al., 2019; Lu et al., 2020a), slumps (Lu et al., 2017; Schnellmann et al., 2002), detachment surfaces (Greene et al., 1994; Zhang et al., 2008), and turbidites (Ghazoui et al., 2019; Lu et al., 2021; Moernaut et al., 2014). Seismites from the Eastern European Alps (Plan et al., 2010) and the northern Bighorn Basin, USA (Jackson et al., 2019) have been used to detect fault activities and regional tectonism. Here, we use a 2-Myr-long seismite record preserved in lacustrine deposits from the crest of the Jianshan Anticline as an example of

deformation within continental blocks between prominent strike-slip faults that dominate the "escape tectonics" in the region (Yin, 2010).

2. The Jianshan Anticline and Core SG-1b

The seismic profile across the Jianshan Anticline shows that it is linked to a shallow blind thrust that developed beneath the paleo-Qaidam Lake floor since the Oligocene (~33 Ma; Figures 1c and 1d), with its deformation rate accelerating since the Miocene (Bally et al., 1986; Liu et al., 2017; Meyer et al., 1998; Wu et al., 2019). During 2011, a 723 m-deep core SG-1b was drilled on the crest of Jianshan Anticline (Figure 1; Text S1). Detailed paleomagnetic dating constrains the age of the generally well-laminated or layered sediments in the core to 7.3-1.6 Ma (Zhang et al., 2014).

The frequent appearance of tempestites, ooid-rich sediments, and undisturbed evaporites in Core SG-1b since 3.6 Ma suggests that the crest of the fold rose above the storm wave base and into a shallow water (few meters-deep) environment since that time, while lacustrine sedimentation did not cease on its crest until 1.6 Ma (Lu et al., 2015, 2020b). The uninterrupted subaqueous sedimentary sequence (~33-1.6 Ma) may therefore have continuously recorded effects of late Cenozoic deformation that propagated from the Indo-Asia collision zone to NE Tibet.

3. Materials, Methods, and Chronology

The studied core section (260-0 m) comprises laminated mud, layered mud, massive mud, mud containing evaporites, and evaporites (Text S2) (Lu et al., 2020b). Paleomagnetic dating constrains the age of the studied core interval to ca. 3.6-1.6 Ma (Zhang et al., 2014). Recently, orbital tuning based on the Rb/Sr record has been conducted on the 183-52 m core interval that is thus more precisely dated at 3.3-2.1 Ma (Kaboth-Bahr et al., 2020) (Figure S1; Table S1). Calculations of sedimentation rates are based on this age-model.

The archived half of Core SG-1b was scanned with the Avaatech 4th generation XRF Scanner (equipped with CCD-Color Line Scan Camera) at a resolution of 1 cm, an exposure time of 10 s (Text S3) (Kaboth-Bahr et al., 2020). A recent study on the Core SG-1b has shown that strontium (Sr) best reflects Ca-bearing minerals (e.g., carbonate or gypsum) (Kaboth-Bahr et al., 2020). In the present study, we therefore also use Sr to investigate the different facies. For the first time, we identify various types of disturbances by using these high-resolution XRF data and images (Figure 2). As the instantaneous events are considered to develop immediately below the water-sediment interface, then the timing of each event is constrained by the age of the first overlying undisturbed sediment horizon and is calculated by linear interpolation.

We specifically chose the upper 260 m of Core SG-1b for our case study because it provides a rare opportunity to identify disturbances and understand regional deformations. First, the core was drilled directly on the crest of a thrust-cored anticline whose geological evolution has been constrained by the seismic reflection profile (Lu et al., 2015). Second, the age of the focused core section has been well constrained by both paleomagnetic dating (Zhang et al., 2014) and orbital tuning (Kaboth-Bahr et al., 2020). Third, the lithology in the core interval of 101-56 m is well-understood (Lu et al., 2020b). Thereby, this unique core section allows a better understanding of various sedimentary processes and the effects that different triggers involved, and thus allows reliable identification of sedimentary imprints of both paleoearthquakes/tectonics and non-earthquakes.

4. Results

4.1. Different Types of Disturbances in Core SG-1b

4.1.1. Type I: Artificial Disturbances

Drilling disturbances are visible in some cored intervals of layered mud (Figures 2e, 2i, and S2h). The disturbances normally extend along the drill direction (from top to bottom) and are best developed toward the edges of the core.

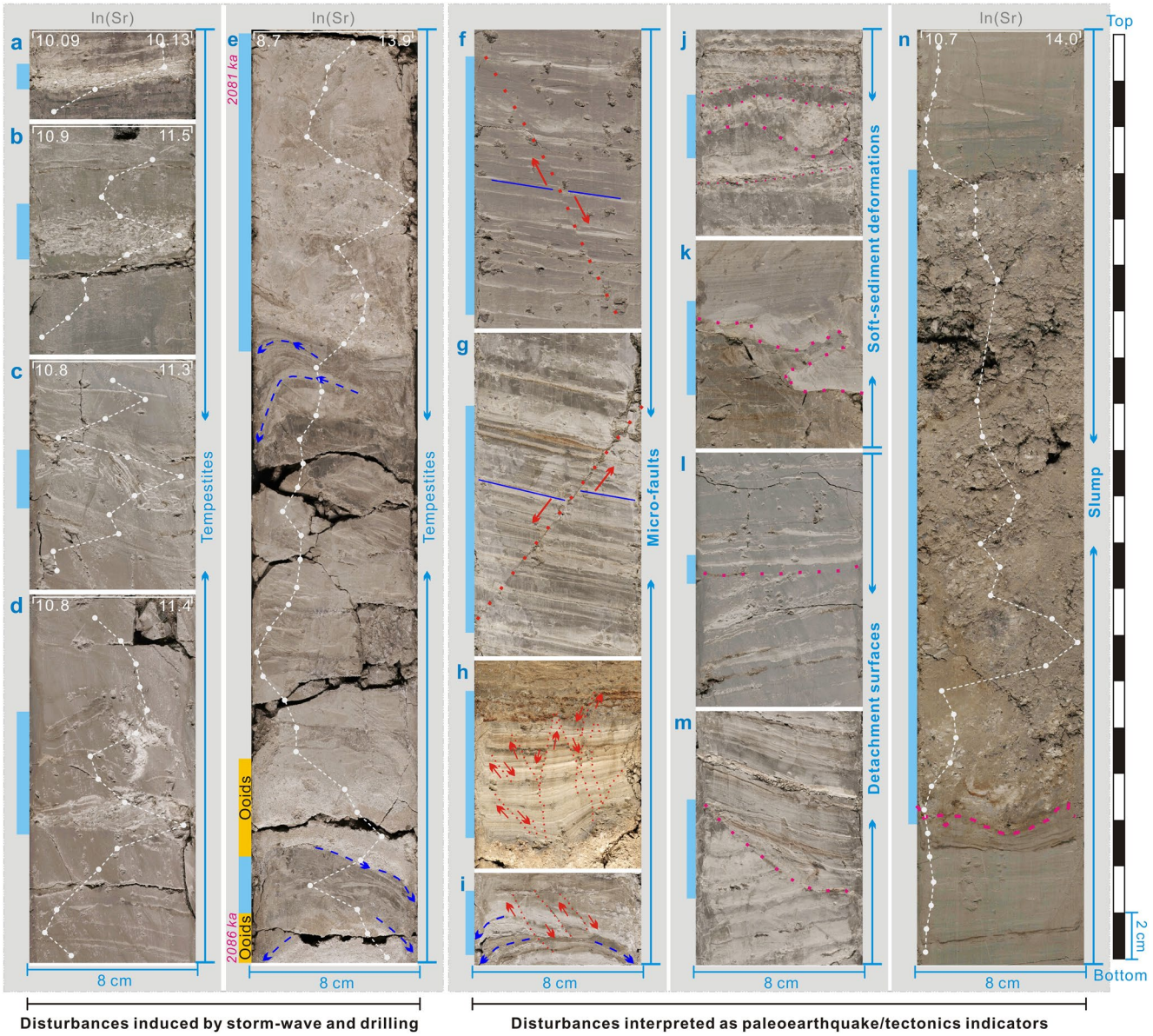

Figure 2. The various types of disturbances in Core SG-1b. The light blue bars indicate the position of events; the white dashed lines and points represent XRF data. (a–e) Disturbances induced by storm-waves and drilling. Note the blue dashed lines in (e) and (i) indicate artificial disturbances (deformation). (f–n) Disturbances are interpreted as paleoearthquake/tectonic indicators. (f, g) Normal faults; the blue lines indicate the correlated marker layers. (h, i) Fault-graded beds; the red dashed lines indicate the positions of the slip plane, while the red arrows indicate slip directions. (j, k) Soft-sediment deformations. (l, m) Detachment surfaces. (n) Slump layer; the pink dashed line indicates the erosive base. See Text S4 for core depth.

4.1.2. Type II: Storm-Wave Induced Disturbances

These disturbances comprise evaporite fragments (high content in Sr) floating in fine sands or mud. They are characterized by the sorting of evaporite fragments and lack distinct erosional bases (Figures 2a–2e and S2).

4.1.3. Type III: Micro-Faults

We identify 31 layers that each contain a single normal fault (Figures 2f and 2g) and 48 fault-graded beds (Figures 2h, 2i, and S3). Fault-graded beds are layers where multiple micro-faults appear. The displacements of these micro-faults are varying from millimeters to centimeters.

4.1.4. Type IV: Soft-Sediment Deformation

These structures are characterized by layer-parallel displacements. All these horizons are observed within core intervals of layered mud and laminations and are capped by overlying layered mud or laminations (Figures 2j and 2k and S4). We identify 34 such disturbances with thicknesses ranging between 3 and 33 cm.

4.1.5. Type V: Slumps

Slumps are characterized by deformed mud-containing evaporites (high content in Sr), deformed laminations, or folding of mud layers (Figures 2n and S5). Erosive or bedding plane detachment surfaces are commonly observed at their base, and thus differentiate slumps from in situ soft-sediment deformation described above. We record 41 slump horizons with thicknesses ranging from 3 to 91 cm.

4.1.6. Type VI: Detachment Surfaces

The structures are characterized by sharp contacts (Figures 2l, 2m, and S6). We identify 10 detachment surfaces in the core.

4.2. Distribution of Type III–VI Disturbances and Sedimentation Rates During 3.6-1.6 Ma

Micro-faults, soft-sediment deformation, and detachment surfaces mainly occur within the core intervals of laminated and layered mud (Figure 3). Slumps however are more commonly preserved within core intervals of massive mud and layered mud. At an orbital-scale, sedimentation rates based on the core are high during 3.6-2.7 Ma (with a mean of 16.5 cm/Kyr), low during 2.1-1.6 Ma (mean: 10.7 cm/Kyr), but are very low during 2.7-1.6 Ma (mean: 7.5 cm/Kyr). We identify a total of 164 such disturbances in the studied section, 126 of them (77%) occurred between 3.6 and 2.7 Ma (255-112 m) (Figure 3).

5. Discussion

5.1. Triggering Mechanisms of Type III–VI Disturbances

5.1.1. Type III: Micro-Faults

Micro-faults are a consequence of brittle deformation caused by a high strain rate (Seilacher, 1969). The micro-faults in Core SG-1b do not result from gravitational loading because (i) they commonly cut through coarse-grained laminations/beds of higher densities (Figures 2f and 2i), (ii) no micro-faults are observed immediately below thick coarse-grained layers, (iii) most micro-faults occur within the cored intervals of laminations and layered mud (Figures 3 and S3) which have a stable vertical density structure and only a small vertical density contrast. In addition, the drilling stress which acted on these unconsolidated soft-sediments during their recovery cannot account for these brittle structures as they are not confined to the edge of the core.

Syn-depositional single micro-faults have been identified on a centimeter-scale from lake sediments in Anatolia (Avşar et al., 2016) and the Alps (Monecke et al., 2004) where they have been correlated to modern or historic earthquakes, and thereby interpreted as seismites. In addition, fault-graded beds have been interpreted as seismites caused by strong earthquake-shaking on gradationally compacted muds in quiet water basins (Seilacher, 1969). The observed micro-faults in Core SG-1b are compatible with these well-understood examples and are therefore also considered to be indicators of paleoearthquakes.

5.1.2. Type IV: Soft-Sediment Deformation

Gravitational instability (Rayleigh-Taylor instability), the mechanism for overloading, is one of the most common driving forces for soft-sediment deformations in subaqueous environments (Owen et al., 2011). In Core SG-1b, soft-sediment deformation underlies layered mud or laminations (Figures 2 and S4). No such deformation is developed immediately beneath thick coarse-grained layers with higher density. The laminated and layered sediments in Core SG-1b consist of stably stratified water-saturated mud in which the density increases with depth, and are thus not susceptible to Rayleigh-Taylor Instability which requires inverted densities.

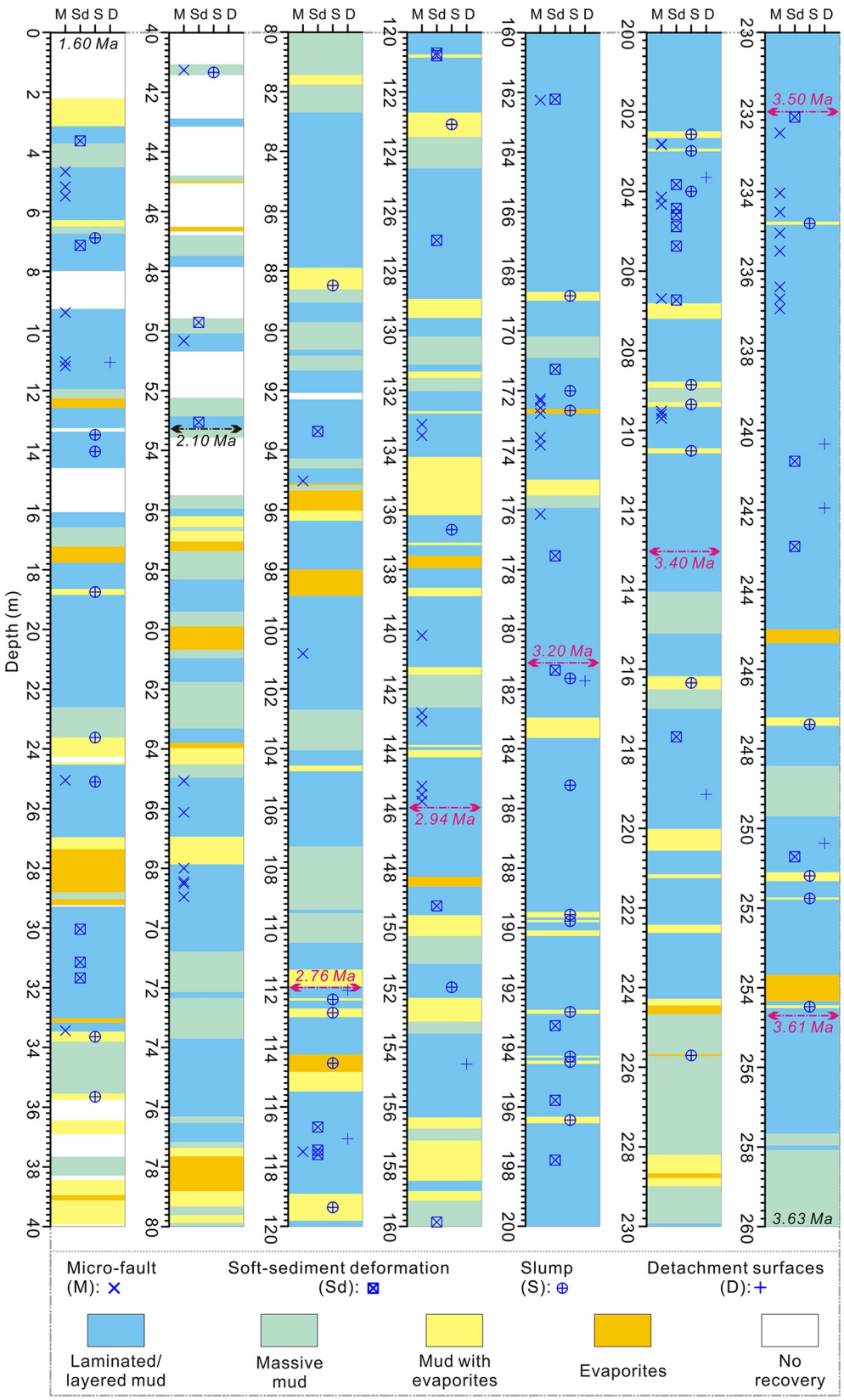

Figure 3. Distribution of Type III–VI disturbances in 260-0 m of Core SG-1b (3.6-1.6 Ma). Micro-faults, soft-sediment deformation, and detachment surfaces have mainly occurred within the core intervals of laminations and layered mud. The coring rate in the upper 56 m is relatively low (~70%) (Zhang et al., 2014).

Another common driving force for soft-sediment deformations in subaqueous environments is storm-waves (Owen et al., 2011). Typical deformation created by storm-waves include load-casts which are commonly associated with tempestites (Molina et al., 1998). In Core SG-1b, the 34 deformed horizons show no association with tempestites. Besides, none of the deformed horizons show a correlation with ooid layers (with high content in Sr) which would indicate that the depositional environment is under the strong influence of waves (Figure 2e). We therefore discard storm-waves as the primary trigger for the 34 deformed horizons. In addition, we suggest that the drilling process cannot account for these deformations because artificial stress mainly acts on the edges of the core. It cannot induce layer-parallel displacements and deformations in the center of the event layer which is constrained by laminations/layered mud at the top and bottom (Figures 2 and S4).

The observed deformation is similar to other soft-sediment structures in lakes from tectonically active regions such as Anatolia (Avşar et al., 2016), South-central Chile (Moernaut et al., 2014), California (Sims, 1973), and the Dead Sea (Ken-Tor et al., 2001). Soft-sediment deformation from these regions has been correlated with instrumental or historic earthquakes with magnitudes ranging from M_w 5.3 to 9.6 and local shaking intensities from >VI to IX, and interpreted as seismites. Previous studies reveal that such seismic-induced deformation occurred immediately below the water-sediment interface (Avşar et al., 2016; Lu et al., 2021; Sims, 1973). There is a lack of erosional bases developed below the deformed layers that would allow us to infer a slump source for these features, and they are therefore considered to be formed in situ. The earthquake-forced shear known as the Kelvin-Helmholtz instability is a plausible driver for the layer-parallel shear during soft-sediment deformations (Heifetz et al., 2005; Lu et al., 2020a; Wetzler et al., 2010). We interpret the observed soft-sediment deformations in Core SG-1b as reflecting seismically triggered shear instability, which can therefore be used as a paleoearthquake indicator.

5.1.3. Type V: Slumps

The common presence of evaporites in slumps makes these layers distinct from the overlying and underlying laminated or layered mud, and implies a shallow water source for the slumps. However, the lack of coarse sands in the slumps, and the high relief of the Jianshan Anticline on the lake floor, do not support a distant lakeshore origin for the evaporites (the regions in front of the Altyn Tagh Range). One viable source for the evaporites is the higher elevations created around the crest of the Jianshan Anticline, where water depth would be shallower and evaporite deposition would increase.

The absence of coarse terrigenous sediment supply, low sedimentation rate, and extremely gentle slope angles (<1°) at the crest of the Jianshan Anticline make non-seismic triggering mechanisms, such as sediment loading or gravitational gliding, highly unlikely. The most plausible triggers for slumps in such a setting (on the crest of an anticline) are earthquakes. A negligible slope angle (<1°) is sufficient for earthquake-triggered subaqueous slope failures (Alsop & Marco, 2013; Field et al., 1982). Slumps triggered by historic earthquakes with magnitudes ranging from M_w 5.9 to 7.5, have been reported from lacustrine environments in the Alpine range (Schnellmann et al., 2002) and British Columbia, Canada (Shilts & Clague, 1992), and interpreted as seismites.

5.1.4. Type VI: Detachment Surfaces

Detachment surfaces in drill cores have been used previously in tectonically active regions to indicate local deformation (Greene et al., 1994; Guo et al., 2005) and paleoearthquakes (Zhang et al., 2008). The coring site is located close to the top of the Jianshan Anticline and we here interpret detachment surfaces preserved in the core as failure surfaces formed toward the head scarp of seismic-induced slumps that translated downslope from the anticlinal crest. Similar gravity-driven bedding-parallel detachment surfaces generated by the downslope-directed failure of sediments have been recently recorded in outcrops from the Dead Sea (Alsop et al., 2020).

5.2. Implications for Paleoearthquake Recurrence Pattern

We interpret micro-faults, soft-sediment deformation, slumps, and detachment surfaces (Type III–VI disturbances) in Core SG-1b as seismites. The entire seismite catalog that spanned 3.6-1.6 Ma comprises 164 such events, and yields a mean event return time of 12.0 Kyr, a standard deviation (STD) of 24.9 Kyr, and

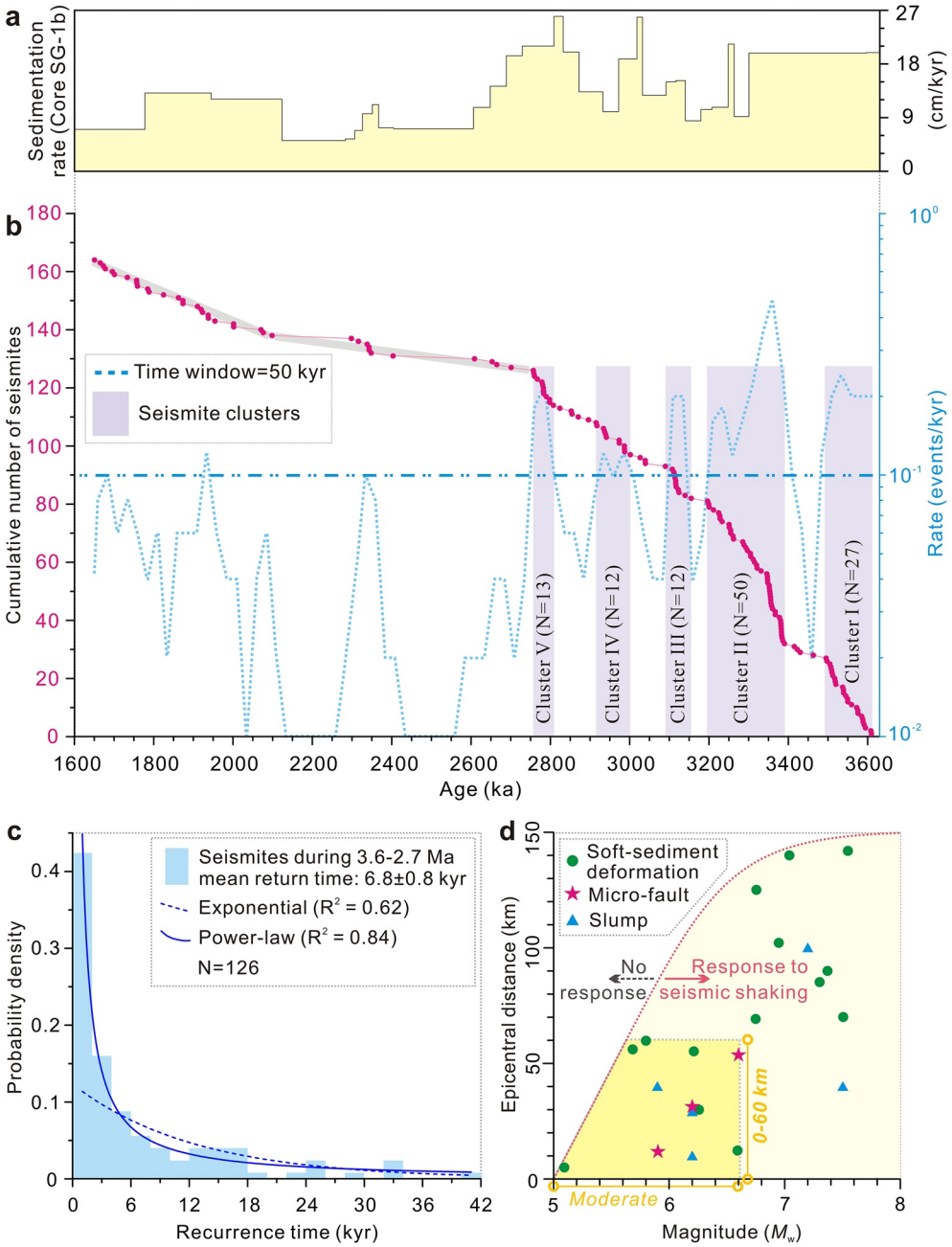

Figure 4. Distribution of seismites during 3.6-1.6 Ma. (a) Sedimentation rate during 3.6-1.6 Ma. (b) Cumulative (red dots) and seismites rate (light blue) over the time interval of the seismite record. (c) Histograms for recurrence times of events during 3.6-2.7 Ma. Exponential and power-law distributions are plotted for comparison. (d) Instrumental and historical earthquake magnitude versus epicentral distance plot based on literature to show thresholds for micro-faults (Avşar et al., 2016; Monecke et al., 2004), soft-sediment deformation (Agnon et al., 2006; Avşar et al., 2016; Moernaut et al., 2014; Sims, 1973), and slumps (Becker et al., 2005; Piper et al., 1988; Schnellmann et al., 2002; Shilts & Clague, 1992; Wilhelm et al., 2016) in subaqueous environments in different regions. The yellow-colored area highlights the seismic effects of moderate earthquakes with epicentral distance ≤60 km.

a coefficient of variation (COV: STD divided by mean) of 2.1. The low coring rate during 2.1-1.6 Ma results in an incomplete part of the seismite record (Figure 3). The relatively low sedimentation rate during 2.7-2.1 Ma might have rendered the sediments less sensitive to seismic shaking, and thus fewer earthquakes were recorded (Figure 4).

In contrast, the seismite record during 3.6-2.7 Ma ($N = 126$) yields a mean recurrence time of 6.8 Kyr and a COV of 1.3. The recurrence times follow a power-law distribution (Figure 4c). The large COV and the power-law distribution of recurrence times suggest the events are clustered in time during 3.6-2.7 Ma. The power-law distribution of recurrence times and the large mean recurrence time (6.8 Kyr) also support the links that we propose between Type III–VI disturbances and paleoearthquakes. This is because the occurrence of non-earthquake triggers and their triggered events are normally more periodic and frequent.

To identify earthquake temporal clusters in the catalog, we compute the seismicity rate using a moving time window of 50 Kyr (≈2*STD), with an overlap of 50%. The calculated seismic rate presents five seismite clusters that are distinguished above the seismicity rate threshold of 0.1 (≈2/STD) (Figure 4b). The five clusters occurred at 3.6-3.5, 3.4-3.2, 3.15-3.1, 3.0-2.9, and 2.8-2.75 Ma, and yield a mean recurrence of 4.4 ± 0.9 (standard error of the mean) Kyr, 4.0 ± 0.7 Kyr, 5.9 ± 2.0 Kyr, 7.8 ± 3.0 Kyr, and 4.2 ± 1.2 Kyr, respectively. Also, we should note that some short time periods with very low sedimentation rates or hiatuses might exist since the drilling site is on the crest of an anticline. We cannot rule out the possibility that some seismites were missed during the quiet periods between the clusters, due to potentially very low sedimentation rates over shorter time periods, or the sediments being less sensitive to seismic shaking.

5.3. Implications for Regional Tectonism

Available Holocene paleoseismic records based on fault trenching from the nearby Xorkoli section (Yuan et al., 2018) and Aksay section (Shao et al., 2018) of the Altyn Tagh Fault indicate a quasi-periodic rupture behavior along the fault (Figures 1b and 1c). The mean recurrence of major earthquakes on these sections are 0.6 Kyr during 6-0 ka and 1.4 Kyr during 8-0 ka, respectively (Shao et al., 2018; Yuan et al., 2018). In addition, previous paleoseismology studies based on terraces indicate that the mean recurrence of M_w 8 earthquakes on the western part of the east Kunlun Fault (≥300 km from Core SG-1b site; Figure 1b) is about 0.9 Kyr during 8-2 ka (Van Der Woerd et al., 2002). Previous studies have also indicated essentially stable deformation rates (~9 mm/yr) in the region along the Altyn Tagh Fault over million years (Yin et al., 2002). These estimated rates are remarkably similar to those established from GPS measurements (Bendick et al., 2000; Chen et al., 2000). So, the Altyn Tagh Fault in this region is more likely to have a quasi-periodic rupture behavior during the past few million years. A mean recurrence of < 0.6 Kyr is expected if the first-order Altyn Tagh Fault and Kunlun Fault are the major sources of recorded paleoearthquakes in Core SG-1b.

However, the smallest mean recurrence of earthquakes of the recorded five clusters in Core SG-1b is 4.0 Kyr, much larger than 1 Kyr. Besides, the extremely high COV value of the SG-1b seismite record suggests that the drilling site was affected by the geometrically complex thrust system that surrounds the anticline. These features imply that the local structures, for example, the Jianshan Anticline and nearby folds (Figure 1c), rather than the Altyn Tagh Fault and/or Kunlun Fault are the major sources. These folds have developed above shallow thrusts beneath the lake floor, with an axial length of 20–50 km, which are capable of triggering moderate earthquakes ($M_w \geq 5.0$).

Previous subaqueous paleoseismology investigations (Agnon et al., 2006; Avşar et al., 2016; Becker et al., 2005; Moernaut et al., 2014; Monecke et al., 2004; Piper et al., 1988; Schnellmann et al., 2002; Shilts & Clague, 1992; Sims, 1973; Wilhelm et al., 2016) suggest that moderate earthquakes with epicentral distance < 60 km are sufficient to induce seismites, for example, soft-sediment deformation (Figure 4d). Therefore, the high COV value and long mean recurrence deduced from Core SG-1b seismite record indicate that the Jianshan Anticline and surrounding folds and thrusts within the western Qaidam Basin are the most plausible major source of the recorded paleoearthquakes.

The paleoseismic record preserved in Core SG-1b records five seismite clusters. The clustered behavior suggests that the rate of tectonic strain accommodated by the Qaidam thrust system varies over time and thereby reveals episodic fold-and thrust deformation in the region. However, previous studies imply the Altyn Tagh Fault in this region is more likely to have a quasi-periodic rupture behavior over the past few million years (Shao et al., 2018; Yin et al., 2002; Yuan et al., 2018). We therefore propose that during the seismite clusters, more deformation is concentrated in the fold-and-thrust system, however, during the intervening quiescent periods, deformation is focused more along the Altyn Tagh and Kunlun strike-slip faults. During

both the seismite clusters and intervening quiescent periods, both systems might have accommodated the same constant far-field tectonic loading induced by the collision.

Similar research has been conducted in the northern Bighorn Basin, USA where Jackson et al. (2019) interpreted the Upper Cretaceous soft-sediment deformations (in the form of clastic dikes) as seismites, and used these to understand the spatial-temporal development of Laramide deformation. Our results from the NE Tibetan Plateau highlight the potential of long-term seismite sequences to detect tectonism and contribute to our understanding of the long-term seismo-tectonic evolution of the active thrust zone. Our innovative sedimentological method to detect regional tectonics may also prove suitable for similar geological settings (tectonically active regions with continuous lacustrine/marine deposits) elsewhere in the world.

Data Availability Statement

Data sets are available in the supporting information and at PANGAEA database (https://doi.org/10.1594/PANGAEA.922852).

Acknowledgments
This research was inspired by Prof. Lin Ding's comments on the doctoral thesis proposal of Yin Lu in May 2014 at the Institute of Tibetan Plateau Research, China. We thank Profs. Todd Ehlers, Erwin Appel, and Oliver Friedrich for fruitful discussions in the early stage of this research. We appreciate the editor Germán Prieto for handling our manuscript, Jérôme Nomade and one anonymous reviewer for constructive reviews. We thank Werner Fielitz for comments, A. Koutsodendris, K. S. Nakajima, and H. Campos for help with lab work, and W. Rösler and H. Schulz for help with core sampling. Financial support was provided by the German Research Foundation (# FR2544/13-1 to O. Friedrich) and the University of Liege under Special Funds for Research, IPD-STEMA Program (R.DIVE.0899-J-F-G to Y. Lu).

References

Agnon, A., Migowski, C., & Marco, S. (2006). Intraclast breccias in laminated sequences reviewed: Recorders of paleo-earthquakes. *Geological Society of America Special Paper*, *401*, 195–214. https://doi.org/10.1130/2006.2401(13)

Alsop, G. I., & Marco, S. (2013). Seismogenic slump folds formed by gravity-driven tectonics down a negligible subaqueous slope. *Tectonophysics*, *605*, 48–69. https://doi.org/10.1016/j.tecto.2013.04.004

Alsop, G. I., Weinberger, R., Marco, S., & Levi, T. (2020). Bed-parallel slip: Identifying missing displacement in mass transport deposits. *Journal of Structural Geology*, *131*, 103952. https://doi.org/10.1016/j.jsg.2019.103952

Avşar, U., Jónsson, S., Avşar, Ö., & Schmidt, S. (2016). Earthquake-induced soft-sediment deformations and seismically amplified erosion rates recorded in varved sediments of Köyceğiz Lake (SW Turkey). *Journal of Geophysical Research: Solid Earth*, *121*(6), 4767–4779. https://doi.org/10.1002/2016JB012820

Bally, A., Chou, I.-M., Clayton, R., Eugster, H., Kidwell, S. M., Meckel, L., et al. (1986). *Notes on sedimentary basins in China: Report of the American sedimentary basins delegation to the People's Republic of China*. Rep. 2331-1258. US Geological Survey.

Becker, A., Ferry, M., Monecke, K., Schnellmann, M., & Giardini, D. (2005). Multiarchive paleoseismic record of late Pleistocene and Holocene strong earthquakes in Switzerland. *Tectonophysics*, *400*(1), 153–177.

Bendick, R., Bilham, R., Freymueller, J., Larson, K., & Yin, G. (2000). Geodetic evidence for a low slip rate in the Altyn Tagh fault system. *Nature*, *404*(6773), 69–72.

Chen, Z., Burchfiel, B., Liu, Y., King, R., Royden, L., Tang, W., et al. (2000). Global Positioning System measurements from eastern Tibet and their implications for India/Eurasia intercontinental deformation. *Journal of Geophysical Research*, *105*(B7), 16215–16227. https://doi.org/10.1029/2000JB900092

Cowgill, E., Gold, R. D., Xuanhua, C., Xiao-Feng, W., Arrowsmith, J. R., & Southon, J. (2009). Low Quaternary slip rate reconciles geodetic and geologic rates along the Altyn Tagh fault, northwestern Tibet. *Geology*, *37*(7), 647–650. https://doi.org/10.1130/g25623a.1

Field, M. E., Gardner, J. V., Jennings, A. E., & Edwards, B. D. (1982). Earthquake-induced sediment failures on a 0.25° slope, Klamath River delta, California, *Geology*, *10*(10), 542–546.

Freund, R. (1965). A model of the structural development of Israel and adjacent areas since upper Cretaceous times. *Geological Magazine*, *102*(3), 189–205.

Ghazoui, Z., Bertrand, S., Vanneste, K., Yokoyama, Y., Nomade, J., Gajurel, A., & van der Beek, P. (2019). Potentially large post-1505 AD earthquakes in western Nepal revealed by a lake sediment record. *Nature Communications*, *10*(1), 2258.

Greene, H. G., Collot, J. Y., Fisher, M. A., & Crawford, A. J. (1994). Neogene tectonic evolution of the New Hebrides island arc: A review incorporating ODP drilling results. *Proceedings of the Ocean Drilling Program, Scientific Results*, *134*, 19–46. https://doi.org/10.2973/odp.proc.sr.134.002.1994

Guo, Z.-J., Yin, A., Robinson, A., & Jia, C.-Z. (2005). Geochronology and geochemistry of deep-drill-core samples from the basement of the central Tarim basin. *Journal of Asian Earth Sciences*, *25*(1), 45–56.

Heifetz, E., Agnon, A., & Marco, S. (2005). Soft sediment deformation by Kelvin Helmholtz instability: A case from Dead Sea earthquakes. *Earth and Planetary Science Letters*, *236*(1–2), 497–504. https://doi.org/10.1016/j.epsl.2005.04.019

Hubert-Ferrari, A., Armijo, R., King, G., Meyer, B., & Barka, A. (2002). Morphology, displacement, and slip rates along the North Anatolian Fault, Turkey. *Journal of Geophysical Research*, *107*(B10), 2235. https://doi.org/10.1029/2001JB000393

Jackson, W. T., McKay, M. P., Bartholomew, M. J., Allison, D. T., Spurgeon, D. L., Shaulis, B., et al. (2019). Initial Laramide tectonism recorded by Upper Cretaceous paleoseismites in the northern Bighorn Basin, USA: Field indicators of an applied end load stress. *Geology*, *47*(11), 1059–1063. https://doi.org/10.1130/g46738.1

Kaboth-Bahr, S., Koutsodendris, A., Lu, Y., Nakajima, K., Zeeden, C., Appel, E., et al. (2020). A late Pliocene to early Pleistocene (3.3–2.1 Ma) orbital chronology for the Qaidam Basin paleolake (NE Tibetan Plateau) based on the SG-1b drillcore record. *Newsletters on Stratigraphy*, *53*(4), 479–496. https://doi.org/10.1127/nos/2020/0555

Ken-Tor, R., Agnon, A., Enzel, Y., Stein, M., Marco, S., & Negendank, J. F. W. (2001). High-resolution geological record of historic earthquakes in the Dead Sea basin. *Journal of Geophysical Research*, *106*(B2), 2221–2234.

Liu, R., Allen, M. B., Zhang, Q., Du, W., Cheng, X., Holdsworth, R. E., & Guo, Z. (2017). Basement controls on deformation during oblique convergence: Transpressive structures in the western Qaidam Basin, northern Tibetan Plateau. *Lithosphere*, *9*(4), 583–594. https://doi.org/10.1130/l634.1

Lu, H., Ye, J., Guo, L., Pan, J., Xiong, S., & Li, H. (2018). Towards a clarification of the provenance of Cenozoic sediments in the northern Qaidam Basin. *Lithosphere*, *11*(2), 252–272. https://doi.org/10.1130/l1037.1

Lu, Y., Dewald, N., Koutsodendris, A., Kaboth-Bahr, S., Rössler, W., Pross, J., et al. (2020b). Sedimentological evidence for pronounced glacial-interglacial climate fluctuations in NE Tibet in the latest Pliocene to early Pleistocene. *Paleoceanography and Paleoclimatology*, *35*(5), e2020PA003864. https://doi.org/10.1029/2020PA003864

Lu, Y., Fang, X., Appel, E., Wang, J., Herb, C., Han, W., et al. (2015). A 7.3-1.6 Ma grain size record of interaction between anticline uplift and climate change in the western Qaidam Basin, NE Tibetan Plateau. *Sedimentary Geology*, *319*, 40–51. https://doi.org/10.1016/j.sedgeo.2015.01.008

Lu, Y., Moernaut, J., Bookman, R., Waldmann, N., Wetzler, N., Agnon, A., et al. (2021). A new approach to constrain the seismic origin for prehistoric turbidites as applied to the Dead Sea Basin. *Geophysical Research Letters*, *48*(3), e2020GL090947. https://doi.org/10.1029/2020GL090947

Lu, Y., Waldmann, N., Ian Alsop, G., & Marco, S. (2017). Interpreting soft sediment deformation and mass transport deposits as seismites in the Dead Sea depocenter. *Journal of Geophysical Research: Solid Earth*, *122*, 8305–8325. https://doi.org/10.1002/2017JB014342

Lu, Y., Wetzler, N., Waldmann, N., Agnon, A., Biasi, G., & Marco, S. (2020a). A 220,000-year-long continuous large earthquake record on a slow-slipping plate boundary. *Science Advances*, *6*, eaba4170.

Métivier, F., Gaudemer, Y., Tapponnier, P., & Meyer, B. (1998). Northeastward growth of the Tibet plateau deduced from balanced reconstruction of two depositional areas: The Qaidam and Hexi Corridor basins, China. *Tectonics*, *17*(6), 823–842.

Meyer, B., Tapponnier, P., Bourjot, L., Metivier, F., Gaudemer, Y., Peltzer, G., et al. (1998). Crustal thickening in Gansu-Qinghai, lithospheric mantle subduction, and oblique, strike-slip controlled growth of the Tibet plateau. *Geophysical Journal International*, *135*(1), 1–47.

Miller, D. D. (1998). Distributed shear, rotation, and partitioned strain along the San Andreas fault, central California. *Geology*, *26*(10), 867–870.

Moernaut, J., Daele, M. V., Heirman, K., Fontijn, K., Strasser, M., Pino, M., et al. (2014). Lacustrine turbidites as a tool for quantitative earthquake reconstruction: New evidence for a variable rupture mode in south central Chile. *Journal of Geophysical Research: Solid Earth*, *119*(3), 1607–1633. https://doi.org/10.1002/2013jb010738

Molina, J., Alfaro, P., Moretti, M., & Soria, J. (1998). Soft-sediment deformation structures induced by cyclic stress of storm waves in tempestites (Miocene, Guadalquivir Basin, Spain). *Terra Nova*, *10*, 145–150.

Monecke, K., Anselmetti, F. S., Becker, A., Sturm, M., & Giardini, D. (2004). The record of historic earthquakes in lake sediments of Central Switzerland. *Tectonophysics*, *394*(1), 21–40.

Owen, G., Moretti, M., & Alfaro, P. (2011). Recognising triggers for soft-sediment deformation: Current understanding and future directions. *Sedimentary Geology*, *235*(3–4), 133–140. https://doi.org/10.1016/j.sedgeo.2010.12.010

Piper, D. J., Shor, A. N., & Clarke, J. E. H. (1988). The 1929 "Grand Banks" earthquake, slump, and turbidity current. *Geological Society of America Special Paper*, *229*, 77–92.

Plan, L., Grasemann, B., Spötl, C., Decker, K., Boch, R., & Kramers, J. (2010). Neotectonic extrusion of the Eastern Alps: Constraints from U/Th dating of tectonically damaged speleothems. *Geology*, *38*(6), 483–486. https://doi.org/10.1130/g30854.1

Schnellmann, M., Anselmetti, F. S., Giardini, D., McKenzie, J. A., & Ward, S. N. (2002). Prehistoric earthquake history revealed by lacustrine slump deposits. *Geology*, *30*(12), 1131–1134.

Seilacher, A. (1969). Fault-graded beds interpreted as seismites. *Sedimentology*, *13*(1–2), 155–159.

Shao, Y., Liu-Zeng, J., Oskin, M. E., Elliott, A. J., Wang, P., Zhang, J., et al. (2018). Paleoseismic investigation of the Aksay Restraining Double Bend, Altyn Tagh Fault, and its implication for barrier-breaching ruptures. *Journal of Geophysical Research: Solid Earth*, *123*(5), 4307–4330. https://doi.org/10.1029/2017JB015397

Shilts, W., & Clague, J. J. (1992). Documentation of earthquake-induced disturbance of lake sediments using subbottom acoustic profiling. *Canadian Journal of Earth Sciences*, *29*(5), 1018–1042.

Sims, J. D. (1973). Earthquake-induced structures in sediments of Van Norman Lake, San Fernando, California. *Science*, *182*(4108), 161–163.

Tapponnier, P. (2001). Oblique stepwise rise and growth of the Tibet plateau. *Science*, *294*(5547), 1671–1677. https://doi.org/10.1126/science.105978

Taylor, M., & Yin, A. (2009). Active structures of the Himalayan-Tibetan orogen and their relationships to earthquake distribution, contemporary strain field, and Cenozoic volcanism. *Geosphere*, *5*(3), 199–214.

Van Der Woerd, J., Tapponnier, P., Ryerson, F. J., Meriaux, A.-S., Meyer, B., Gaudemer, Y., et al. (2002). Uniform postglacial slip-rate along the central 600 km of the Kunlun Fault (Tibet), from ^{26}Al, ^{10}Be, and ^{14}C dating of riser offsets, and climatic origin of the regional morphology. *Geophysical Journal International*, *148*(3), 356–388.

Wang, M., & Shen, Z. K. (2020). Present-day crustal deformation of continental China derived from GPS and its tectonic implications. *Journal of Geophysical Research: Solid Earth*, *125*(2), e2019JB018774. https://doi.org/10.1029/2019JB018774

Wetzler, N., Marco, S., & Heifetz, E. (2010). Quantitative analysis of seismogenic shear-induced turbulence in lake sediments. *Geology*, *38*(4), 303–306. https://doi.org/10.1130/g30685.1

Wilhelm, B., Nomade, J., Crouzet, C., Litty, C., Sabatier, P., Belle, S., et al. (2016). Quantified sensitivity of small lake sediments to record historic earthquakes: Implications for paleoseismology. *Journal of Geophysical Research: Earth Surface*, *121*(1), 2–16. https://doi.org/10.1002/2015jf003644

Wu, L., Lin, X., Cowgill, E., Xiao, A., Cheng, X., Chen, H., et al. (2019). Middle Miocene reorganization of the Altyn Tagh fault system, northern Tibetan Plateau. *Geological Society of America Bulletin*, *131*(7–8), 1157–1178. https://doi.org/10.1130/b31875.1

Yin, A. (2010). Cenozoic tectonic evolution of Asia: A preliminary synthesis. *Tectonophysics*, *488*(1–4), 293–325. https://doi.org/10.1016/j.tecto.2009.06.002

Yin, A., Dang, Y. Q., Zhang, M., Chen, X. H., & McRivette, M. W. (2008). Cenozoic tectonic evolution of the Qaidam basin and its surrounding regions (Part 3): Structural geology, sedimentation, and regional tectonic reconstruction. *Geological Society of America Bulletin*, *120*(7–8), 847–876. https://doi.org/10.1130/b26232.1

Yin, A., Rumelhart, P. E., Butler, R., Cowgill, E., Harrison, T. M., Foster, D. A., et al. (2002). Tectonic history of the Altyn Tagh fault system in northern Tibet inferred from Cenozoic sedimentation. *Geological Society of America Bulletin*, *114*(10), 1257–1295. https://doi.org/10.1130/0016-7606(2002)114<1257:thotat>2.0.co;2

Yuan, D., Ge, W., Chen, Z., Li, C., Wang, Z., Zhang, H., et al. (2013). The growth of northeastern Tibet and its relevance to large-scale continental geodynamics: A review of recent studies. *Tectonics*, *32*(5), 1358–1370. https://doi.org/10.1002/tect.20081

Yuan, Z., Liu-Zeng, J., Wang, W., Weldon, R. J., Oskin, M. E., Shao, Y., et al. (2018). A 6000-year-long paleoseismologic record of earthquakes along the Xorkoli section of the Altyn Tagh fault, China. *Earth and Planetary Science Letters*, *497*, 193–203. https://doi.org/10.1016/j.epsl.2018.06.008

Zhang, S., Wang, D., Liu, X., Zhang, G., Zhao, J., Luo, M., et al. (2008). Using borehole core analysis to reveal Late Quaternary paleoearthquakes along the Nankou-Sunhe Fault, Beijing. *Science in China - Series D: Earth Sciences*, *51*(8), 1154–1168.

Zhang, W., Appel, E., Fang, X., Song, C., Setzer, F., Herb, C., & Yan, M. (2014). Magnetostratigraphy of drill-core SG-1b in the western Qaidam Basin (NE Tibetan Plateau) and tectonic implications. *Geophysical Journal International*, *197*(1), 90–118. https://doi.org/10.1093/gji/ggt439